Freie Universität Berlin
Department of Physics
Arnimallee 14
14195 Berlin

WS 2011/12

Advanced Lab Course for Master Students
Report

Ma7 - Raman Scattering

Stefanie Kreft
kreft@physik.fu-berlin.de

Samuel Sanchez Viveros
sanchez@physik.fu-berlin.de

November 26, 2011

Tutor: Ph. Klar

Contents

1. Theoretical Background

The development of the Laser enabled the use of Raman scattering as spectroscopic method for the measurement of elementary excitations in solids. The inelastic scattering of photons from an atom or molecule, which is called Raman scattering, is a minor process compared to the elastic scattering of the photons (Rayleigh scattering). This inelastic scattering yields a different frequency of the photons before and after scattering, with the energy difference resulting from the creation or annihilation of a phonon or magnon. The term Raman scattering usually refers to the processes where the scattering leads to a creation/annihilation of optical phonons. The similar process with acoustic phonons is called Brillouin scattering [1]. The macroscopic theory of Raman scattering will be presented in section 1.1 and the microscopic theory in section 1.2. Generally, for Raman scattering and all other scattering processes on periodic structures changing in time, the conservation of energy and momentum have to be fulfilled. This leads to the selection rules

$$\omega = \omega_i \pm \omega_0 \tag{1.0.1}$$

$$\vec{k} = \vec{k_i} \pm \vec{q} + \vec{G} \tag{1.0.2}$$

where ω and $\vec{k}$ belong to the incident phonon, ω_i and $\vec{k_i}$ to the scattered phonon and ω_0 and $\vec{q}$ to the phonon. $\vec{G}$ is a reciprocal lattice vector. For photons in the range of visible light, the wave vector of the incident and scattered photon are approx. 1/1000 of the reciprocal lattice vector. Thus only excitations close to the center of the Brillouin zone occur and the reciprocal wave vector in 1.0.2 is negligible. [2].

1.1. Macroscopic Theory

The interaction of light and a solid with the electric susceptibility χ is sustained by the polarisation of the valence electrons. An incoming electromagnetic field of the form

$$\vec{F}(\vec{r}, t) = \vec{F_i}(\vec{k_i}, \omega_i) \cos(\vec{k_i}\vec{r} - \omega_i t) \tag{1.1.1}$$

induces a polarisation $\vec{P}(\vec{r}, t) = \chi \cdot \vec{F}(\vec{r}, t)$ via the susceptibility tensor χ, which can be treated as an scalar for isotropic media.

$$\vec{P}(\vec{r}, t) = \vec{P}(\vec{k_i}, \omega_i) \cos(\vec{k_i}\vec{r} - \omega_i t) \tag{1.1.2}$$

where the amplitude $\vec{P}(\vec{k}_i, \omega_i)$ is defined as

$$\vec{P}(\vec{k}_i, \omega_i) = \chi(\vec{k}_i, \omega_i)\vec{F}_i(\vec{k}_i, \omega_i). \tag{1.1.3}$$

For finite temperatures, χ fluctuates due to thermally excited atomic vibrations. Atomic displacements $\vec{Q}(\vec{r}, t)$ can be expressed via plane waves with wave vector $\vec{q}$ and frequency ω_0. In the adiabatic approximation, the electronic frequencies are assumed to be larger than ω_0 and therefore the susceptibility can be written as a function of the displacement only. A Taylor expansion of the susceptibility in terms of $\vec{Q}$ yields a term χ_0 independent of $\vec{Q}$ and thereby denoting a system without fluctuations. Terms of higher order represent the oscillations of the susceptibility due to the lattice wave $\vec{Q}$. Thus the polarisation of a medium in presence of atomic vibrations can be expressed as

$$\vec{P}(\vec{r}, t, \vec{Q}) = \vec{P}_0(\vec{r}, t) + P_{ind}(\vec{r}, t, \vec{Q}) \tag{1.1.4}$$

where $\vec{P}_0(\vec{r}, t) = \chi_0\vec{F}(\vec{r}, t)$ and $P_{ind}(\vec{r}, t, \vec{Q}) = (\partial\chi/\partial\vec{Q})_0\vec{Q}(\vec{r}, t)\vec{F}(\vec{r}, t)$. The latter one is induced by the phonon. The definition can be rewritten as

$$\begin{aligned} P_{ind}(\vec{r}, t, \vec{Q}) = \frac{1}{2}(\partial\chi/\partial\vec{Q})_0\vec{Q}(\vec{q}, \omega_0)\vec{F}_i(\vec{k}_i, \omega_i t) \\ \left[\cos\left[(\vec{k}_i + \vec{q})\vec{r} - (\omega_i + \omega_0)t\right]\right. \\ \left. + \cos\left[(\vec{k}_i - \vec{q})\vec{r} - (\omega_i - \omega_0)t\right]\right] \end{aligned} \tag{1.1.5}$$

Thus the induced polarisation consists of two waves with shifted wave vectors and frequencies [3]. Both shifts are identical to the selection rules in (1.0.1) and (1.0.2) which were gained by the conservation laws. The radiation which is produced by this polarisation is known as *Stokes* and *anti-Stokes* wave, the latter referring to the wave with increased energy and momentum. The difference between the incident and scattered photon frequency is called Raman shift. A plot of a Raman spectrum is shown in figure 1.1. During the Stokes process, a phonon is created by the interaction of the incoming radiation with the medium. The anti-Stokes process results in a annihilation of a phonon. Thus, for the latter, a phonon has to exist in order to be annihilated. Therefore the anti-Stokes process requires a temperature larger than 0K in order to occur. For a non-isotropic medium, the Ramam tensor can be written as

$$\vec{R} = \left(\frac{\partial\chi}{\partial Q}\right)_0 \hat{\vec{Q}}(\vec{r}, t) \tag{1.1.6}$$

where $\hat{\vec{Q}}$ is the unit vector in direction of the lattice displacement. With this definition, the intensity of the Raman scattering is proportional to

$$I \propto \left|\vec{e}_i\vec{R}\vec{e}_s\right|^2 \tag{1.1.7}$$

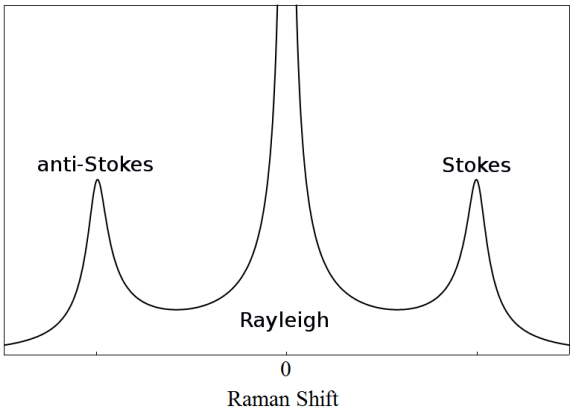

Fig. 1.1.: Raman spectrum [5]

where $\vec{e}_{i/s}$ denote the unit vectors of the polarisation of incoming and scattered light [5]. By measuring the intensity and analyzing its dependence on the incident and scattered polarisation, the symmetry of the Raman tensor and thereby of the phonon, can be deduced. The intensities of the two Raman processes can be calculated via the occupation numbers and the Planck distribution $\langle n_{\vec{k}} \rangle$ and a relation between the two intensities can be derived

$$\frac{I_{Anti-Stokes}}{I_{Stokes}} = \frac{\langle n_{\vec{k}} \rangle}{\langle n_{\vec{k}} + 1 \rangle} = e^{-\frac{\hbar\omega_0}{k_B T}} \text{ [4]}. \tag{1.1.8}$$

1.2. Microscopic Theory

For the microscopic theory, the excitation of an electron by the scattering process is considered. This electron excitation is caused by the incoming photon and can be described by an electron-hole pair, which then interacts with the lattice and results in a new state. Both electron excitation states can be seen es an intermediate states. The second intermediate state decays radiatively and a photon is emitted. The transition rate for the most interesting possibility of transition can be calculated by Fermi's Golden rule, yielding

$$\Gamma_{\omega_i \to \omega_f} = \frac{2\pi}{\hbar} \left| \frac{\langle 0 | H_{e-r} | a \rangle \langle a | H_{e-ion} | b \rangle \langle b | H_{e-r} | 0 \rangle}{(\hbar\omega_i - E_a + i\Gamma)(\hbar\omega_s - E_b + i\Gamma)} \right|^2 \tag{1.2.1}$$

where $|a\rangle$ and $|b\rangle$ are electronic states, $E_{a/b}$ are eigenenergies, Γ inverse of the lifetime of the excited state and H_i the Hamiltonian of electron-radiation interaction and electron-phonon interaction [3]. The Feynman diagram for the Stokes process are shown in Fig. 1.2. For the anti-Stokes process, the diagrams have to be inverted.

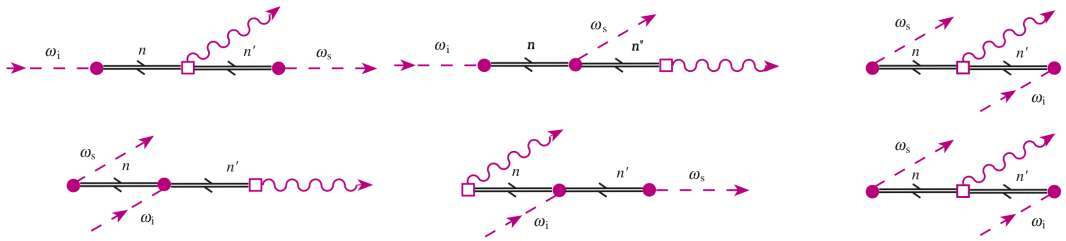

Fig. 1.2.: Feynman diagram of the Raman process [3]

1.3. Problems

1.3.1. Raman peak of Si(111)

For a Raman shift of $\lambda^{-1} = 521 cm^{-1}$, the energy of the corresponding phonon is given as

$$E_P = \hbar\omega = 2\,\pi\,\hbar\,c\,\lambda^{-1} \approx 0,065 eV. \tag{1.3.1}$$

The thermal energy at room temperature is given as

$$E_{Th} = k_B\,T \approx 0,026 eV. \tag{1.3.2}$$

Thus the energy of the phonon is larger than thermal energy, which determines the necessary energy for the anti-Stokes process, because the according phonons have to be annihilated. The Stokes line is far more intense at room temperature. According to (1.1.8), the intensity of the anti-Stokes line increases with temperature, whereas the intensity of the Stokes lines increases with decreasing temperature.

1.3.2. Phonon dispersion

The momentum and wavenumber of a photon with $\lambda = 532 nm$ are given as

$$\left|\vec{k}\right| = \frac{2\pi}{\lambda} = 118104,99 cm^{-1} \tag{1.3.3}$$

$$|\vec{p}| = \hbar \left|\vec{k}\right| = 1,246 \cdot 10^{-27} Ns \tag{1.3.4}$$

The size of the Brillouin zone in reciprocal space is $k_{BZ} = 2\pi/a = 115712436,6 cm^{-1}$ and thus drastically larger than the wave vector. The photon is therefore close to the middle of the Brillouin zone. This is also visible if figure (1.3) is considered. The dispersion of a photon is given as $\omega = ck$, leading to a rather large slope in the dispersion plot. The dispersion of an optical phonon increases significantly slower, the only intersection of the two dispersion relations and therefore the only point for interaction, close to the Brillouin zone middle.

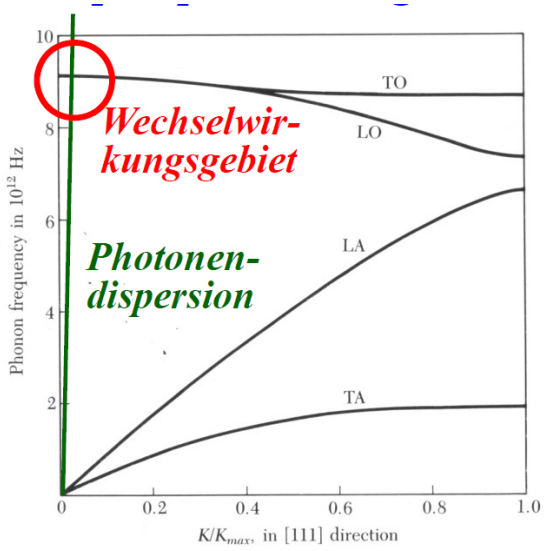

Fig. 1.3.: Dispersion relation for phonon and photons [4]

1.3.3. Peak Positions

From the energy conversation ($E_{RPi} = 2\,\pi\,\hbar\,c\,\lambda^{-1} = E_{Ex} \pm E_{Shi}$) one can conclude $\lambda_{RPi} = (\lambda_{Ex}^{-1} \pm \lambda_{Shi}^{-1})^{-1}$ and calculate the position of the peaks for Si, CaF_2 and graphite as shown in table 1.3.3.

Medium	λ_{Shi}^{-1} in cm^{-1}	λ_{Stokes} in nm	$\lambda_{Anti-Stokes}$ in nm
Si	521	547	518
CaF_2	321	541	523
graphite G-peak	1580	581	491

Tab. 1.1.: Position of the Raman peaks in the spectrum for an excitation wave length of $\lambda_{Ex} = 532nm$.

2. Experimental Setup and Procedure

2.1. Experimental Setup

A sketch of the experimental setup can be found in Fig. 2.1. The photons for the scattering process were emitted by a diode laser with a wavelength of 532 nm. The laser beam was focused onto the sample by a combination of three mirrors and a prism. As samples Si, CaF_2 and a graphite G-peak were used. The reflected incoherent beam was collimated by the first lens and focused into the fiber entrance by a second lens. Between the second lens and fiber entrance a notch filter was installed, which transmitted the Raman scattered wavelength unaltered and weakened the Rayleigh scattered beam by a factor of $(10^5 - 10^6)$[1] in order to be able to resolve the less intense Raman scattered light. The fiber was connected to a spectrometer, where a blazed grating was used to disperse the beam. The spectra were detected by a CCD camera and analyzed with a connected computer. The prism casted a shadow in the beam profile of the scattered light due to the fact that it was inside the beam path. Therefore, the dimensions of the prism were as small as possible to minimize the losses.

2.2. Experimental Procedure

The adjustment of the setup was the crucial part of the experiment. The Raman shifted peaks are only visible for an exact adjustment of the components. Especially the fiber has to be aligned faultlessly to guarantee all information to be transmitted to the spectrometer. Therefore, we adjusted the optical path in such a way, that the sample and the fiber were placed in the focus of the lenses and the beam hit both of them orthogonal. The mirrors and the prism were adjusted to maximize the clearly visible Rayleigh scattered peak at 532 nm. Thus we wanted to perfect the setup and obtain an image of the Raman shifted peaks. Unfortunately, we were not able to detect any shifted peak for any sample. For the analysis we therefore used the data gained by another group. According to their data, the spectra were recorded using a total integration time of 60 s.

[1] optical density of 5-6 according to [5]

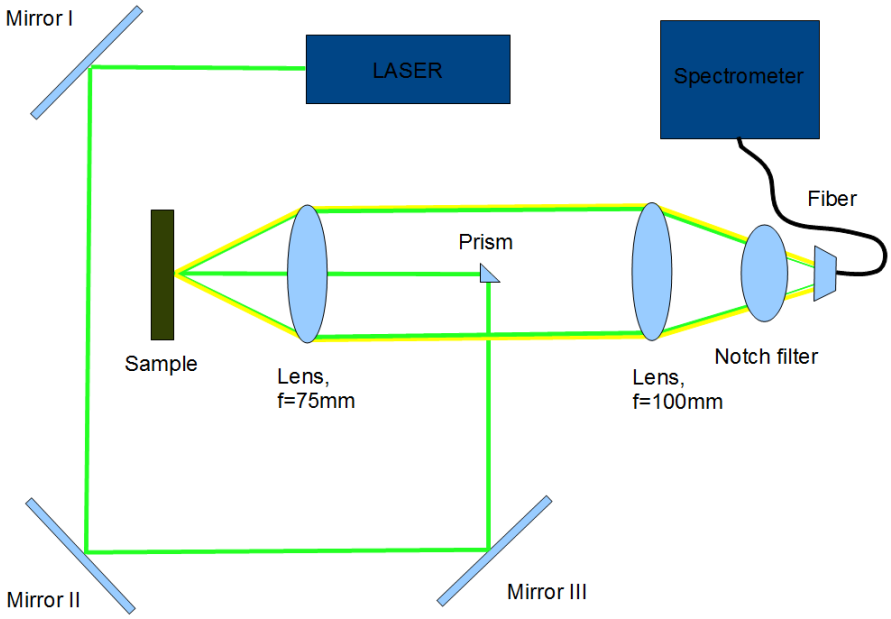

Fig. 2.1.: Experimental Setup

3. Experimental Results and Analysis

The intensity of the Rayleigh peaks for all three data sets being equally approx. 16000 counts and the flat top of the peak suggest, that the CCD-chip was saturated and the peaks were cut off. Therefore, the curves were fitted with a Lorentzian function via `NonlinearModelFit` of MATHEMATICA using

$$I(\lambda; \lambda_0, \Delta\lambda, I_0) = \frac{I_0}{1 + \left(\frac{\lambda - \lambda_0}{\Delta\lambda}\right)^2} + c\,, \tag{3.0.1}$$

where λ_0 denotes the central wavelength, $\Delta\lambda$ the full width at half maximum, I_0 the peak intensity and c the background noise. A Lorentzian function was used due to the Lorentzian shape of the pulses. To extrapolate the peak intensity of the Rayleigh peak we fitted the flanks of the measured peak and calculated the total intensity by integrating with $c = 0$ (i.e. without background noise). This was also done to determine the total intensity of the shifted peaks. The error of the total intensity was estimated from the errors of the parameters used in the numerical calculation as 5%. The errors of the wavelength were taken as the full width half maximum of the Lorentzian fit.

3.1. Spectrum of Si(111)

The spectrum of Silicon can be found in Fig. 3.1. It shows the Rayleigh, first order Stokes and anti-Stokes and second order Stokes peak. The fit of the peaks with the Lorentzian function and the fit parameters can be found in appendix A. The position and intensities of the peaks are given in table 3.1.

The Rayleigh peak is located at $\lambda_R = (532.0 \pm 0.3)nm$, thus as expected at the

process	λ_0 [nm]	I_{tot} [count]
Rayleigh	532.0 ± 0.3	$(1.1 \pm 0.1) \cdot 10^5$
1^{st} Order Stokes	547.2 ± 0.2	2300 ± 115
2^{nd} Order Stokes	560.8 ± 1.3	860 ± 43
Anti-Stokes	517.7 ± 0.2	340 ± 17

Tab. 3.1.: Position and intensities of the Rayleigh, Stokes and anti-Stokes peak of of Si(111)

same wavelength as the incoming photons. The Stokes peak can be found at $\lambda_S = (547.2 \pm 0.2)nm$, shifted by $\Delta\lambda_S = (15 \pm 0.4)nm$ from the Rayleigh peak. The Anti-Stokes peak is shifted by $\Delta\lambda_{aS} = (14.3 \pm 0.4)nm$ to $\lambda_{aS} = (517.7 \pm 0.2)nm$.

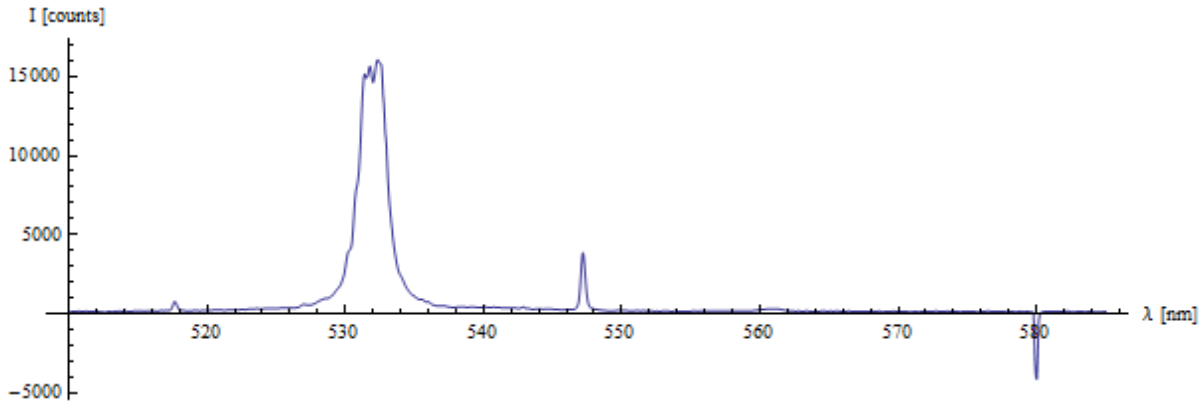

Fig. 3.1.: Spectrum of Silicon

Using this shifts in wavelength to determine the phonon energy yield $E_{Ph} = (64.5 \pm 2.8)meV$, averaged over the slightly different values for the Stokes and Anti-Stokes process. The wavenumber of the Raman shift is given as $\lambda^{-1} = (520.7 \pm 18.0)cm^{-1}$ again averaged for Stokes and anti-Stokes process.
The Stokes peak in second order was also visible at $\lambda_{S,2nd} = 560.8 \pm 1.3$, however with a low intensity. The energy of the phonons in second order is $E_{Ph,2nd} = (119.68 \pm 4.9)meV$, which is within errors twice the energy determined by the first order Stokes peak and thus the energy of two phonons.
The ratio between the intensities of the Stokes and anti-Stokes peak and Stokes and Rayleigh peak respectively were calculated from the values shown in table 3.1.
The ratio between Stokes and anti-Stokes intensity χ_{a-S} was found to be $\chi_{a-S} = 0.15 \pm 0.01$. According to (1.1.8), this leads to a temperature of the sample of $T = (388 \pm 13)K$.
For the ratio between the intensity of the Stokes and the Rayleigh peak χ_{S-R}, the reduction of the intensity of the Rayleigh peak through the Notch filter had to be taken into account, leading to a ratio of χ_{S-R} in the range of $10^{-7} - 10^{-8}$. The large error of the value is due to the imprecise value of the optical density of the Notch filter.

3.2. Spectrum of Graphite

The spectrum of Graphite can be found in Fig. 3.2. It shows the Rayleigh and the first order Stokes peak. The fit of the peaks with the Lorentzian function and the fit parameters can be found in appendix B. The position and intensities of the peaks are given in table 3.2.

The wavelength of the incoming photons equals the wavelength of the Rayleigh peak. The Stokes peak is located at $\lambda_S = (580.0 \pm 0.2)nm$, the Anti-Stokes peak could not be determined, because the range of measurement of the spectrometer was too small. However, it is to expect that due to the low intensity of the Stokes peak, the Anti-Stokes

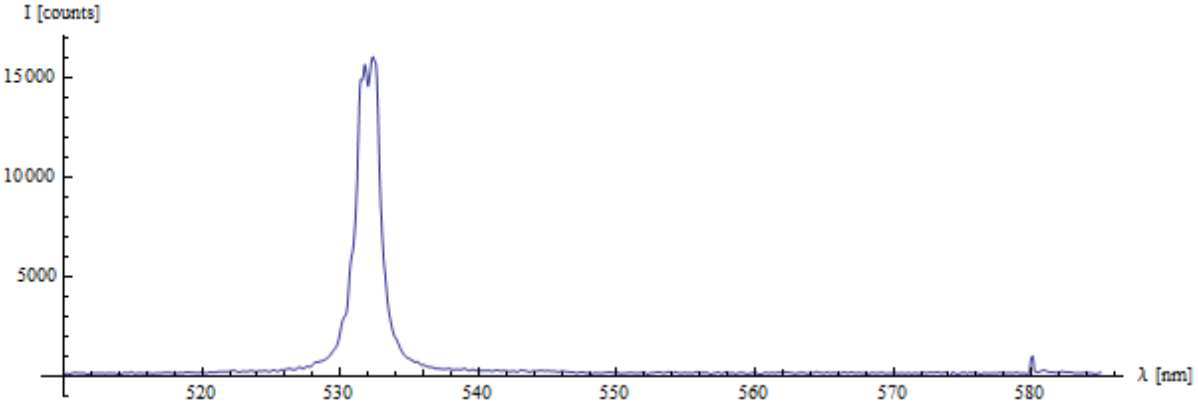

Fig. 3.2.: Spectrum of Graphit

process	λ_0 [nm]	I_{tot} [count]
Rayleigh	532.0 ± 0.3	$(1.0 \pm 0.1) \cdot 10^5$
Stokes	580.0 ± 0.2	370 ± 19

Tab. 3.2.: Position and intensities of the Rayleigh and Stokes peak of Graphite

peak would not have been visible.
The determined phonon energy is $E_{Ph} = (192.9 \pm 1.1)meV$ and the corresponding wavenumber is $\lambda^{-1} = (1555.6 \pm 8.8)cm^{-1}$.
The ratio between the intensities of the Stokes and the Rayleigh peak χ_{S-R} is in the range of $10^{-8} - 10^{-9}$ obtained as before using the optical density of the Notch filter for the determination of the intensity of the Rayleigh peak and thus creating the large error margin.

3.3. Spectrum of CaF_2

The spectrum of CaF_2 can be found in Fig. 3.3. It shows the Rayleigh and first order Stokes and anti-Stokes peak. The fit of the peaks with the Lorentzian function and the fit parameters can be found in appendix C. The position and intensities of the peaks are given in table 3.3.

The wavelength of the incoming photons equals the wavelength of the Rayleigh peak. The Stokes peak is located at $\lambda_S = (541.3 \pm 0.3)nm$, the Anti-Stokes peak is located at $\lambda_{aS} = (523.1 \pm 0.3)nm$. The phonon energy is given as $E_{Ph} = (39.9 \pm 2.2)meV$ and the corresponding wavenumber as $\lambda^{-1} = (321.4 \pm 18.1)cm^{-1}$. Calculating the ratio between the intensities of Stokes and anti-Stokes process yield $\chi_{a-S} = 0.23 \pm 0.02$. This leads to a sample temperature of $T = (315 \pm 12)K$.
The ratio between the intensities of the Stokes and the Rayleigh peak χ_{S-R} is in the

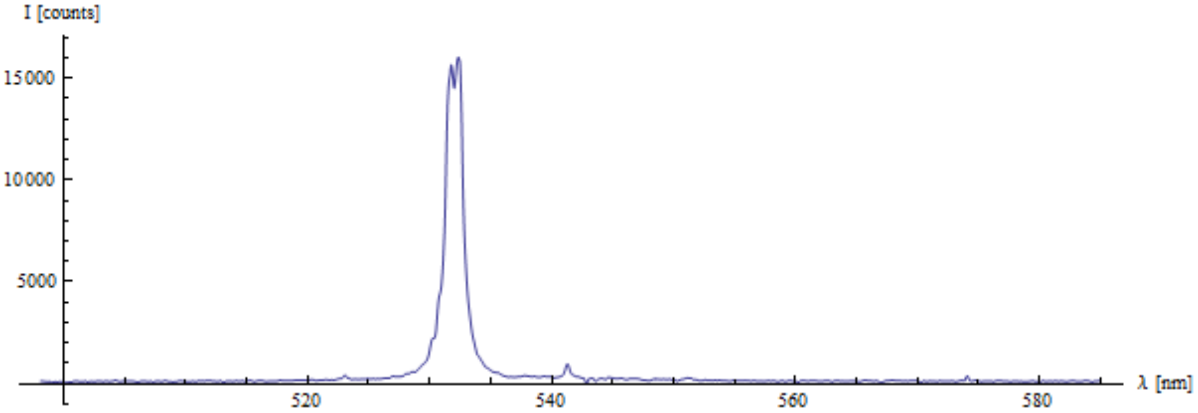

Fig. 3.3.: Position and intensities of the Rayleigh, Stokes and anti-Stokes peak of CaF_2

process	λ_0 [nm]	I_{tot} [count]
Rayleigh	532.0 ± 0.2	$(2.3 \pm 0.2) \cdot 10^5$
Stokes	541.3 ± 0.3	465 ± 24
Anti-Stokes	523.1 ± 0.3	107 ± 6

Tab. 3.3.: Spectrum of CaF_2

range of $10^{-8} - 10^{-9}$ obtained as before using the optical density of the Notch filter for the determination of the intensity of the Rayleigh peak and thus creating the large error margin.

3.4. Influence of bandgap and photon energy on the transition rate

The intensity of the Stokes and Anti-Stokes peak depend among other factors, on the photon energy and the width of the bandgap. It is possible to deduce the electronic band structure of the sample by changing the photon energy systematically. The transition rate between two states, calculated via Fermi's Golden Rule, usually consists of a sum over all possible intermediate and final state combinations, which makes it impossible to deduce the electronic structure of the system. However, if one transition process is resonant and dominates the transition, information of the electronic structure can be obtained. If this is the case, only on term in the sum in Fermi's Golden rule must be considered yielding (1.2.1). This transition process corresponds to the first Feynman diagram in Fig. 1.2. This is the case, if one of the involved intermediate states is real and thus the damping constant $\Gamma \propto \tau_{\text{life}}^{-1}$ is sufficiently small and the energy of the the incoming photon equals the energy of the first intermediate state $|a\rangle$ or the energy of the outgoing photon equals the energy of the second intermediate state $|b\rangle$ respectively.

Three different cases can be distinguished via different magnitudes of lifetime. First, the intermediate state lays in the bandgap and is therefore a virtual state which has according to Heisenberg's uncertainty principle $\tau_{\text{life}} \cdot \Delta E \geq \frac{\hbar}{2}$ a short lifetime. Second, the intermediate state is real. It can either lay the valence band therefore having a lifetime larger than virtual states, but due to thermalization effects will decay with time to the band edge. Third, the state is exactly at the band edge of the valence band, thus leading to the largest possible lifetime. Additionally to the existence of a real state, the energy term in the denominator in (1.2.1) has to vanish to lead to a resonant intensity. This constrictions lead to many possibilities for the Raman process, six of them are shown in Fig. 3.4.

In the first case (cf. Fig. 3.4 (a)), the energy of the incoming photon and of the incoming photon together with the energy of the scattered phonon respectively is smaller than the bandgap. Thus, both intermediate states are virtual and the intensity of the Stokes and anti-Stokes peak is small, because no resonance occurs. In this case, all of the six shown Feynman diagrams contribute equally to the intensity of the peaks.
For an energy of the incoming photon of $\hbar\omega_i = E_g - E_{Phonon}$ (cf. Fig. 3.4 (b)), state $|a\rangle$ is virtual and state $|b\rangle$ for the anti-Stokes process is real. The denominator of the transition equation vanishes for this constellation and leads to resonance for the anti-Stokes process.

Resonance of the Stokes process is achieved, if the energy of the incoming photon is $\hbar\omega_i = E_g + E_{Phonon}$ (cf. Fig. 3.4 (c)). Thus, the state $|b\rangle$ for the Stokes process is real and the denominator vanishes due to the appropriate energy.
For the case of $\hbar\omega_i = E_g$ (cf. Fig. 3.4 (d)), the Stokes and the anti-Stokes process are resonant due to the fact, that state $|a\rangle$ is real and the energy term in the denominator vanishes.

An other possibility for the energy of the incoming photon leads to intermediate states or one intermediate state respectively for the anti-Stokes process within the valence band, which are not resonant, but have a higher intensity than intermediate states within the bandgap due to the increased lifetime (cf. Fig. 3.4 (e)/(f)).

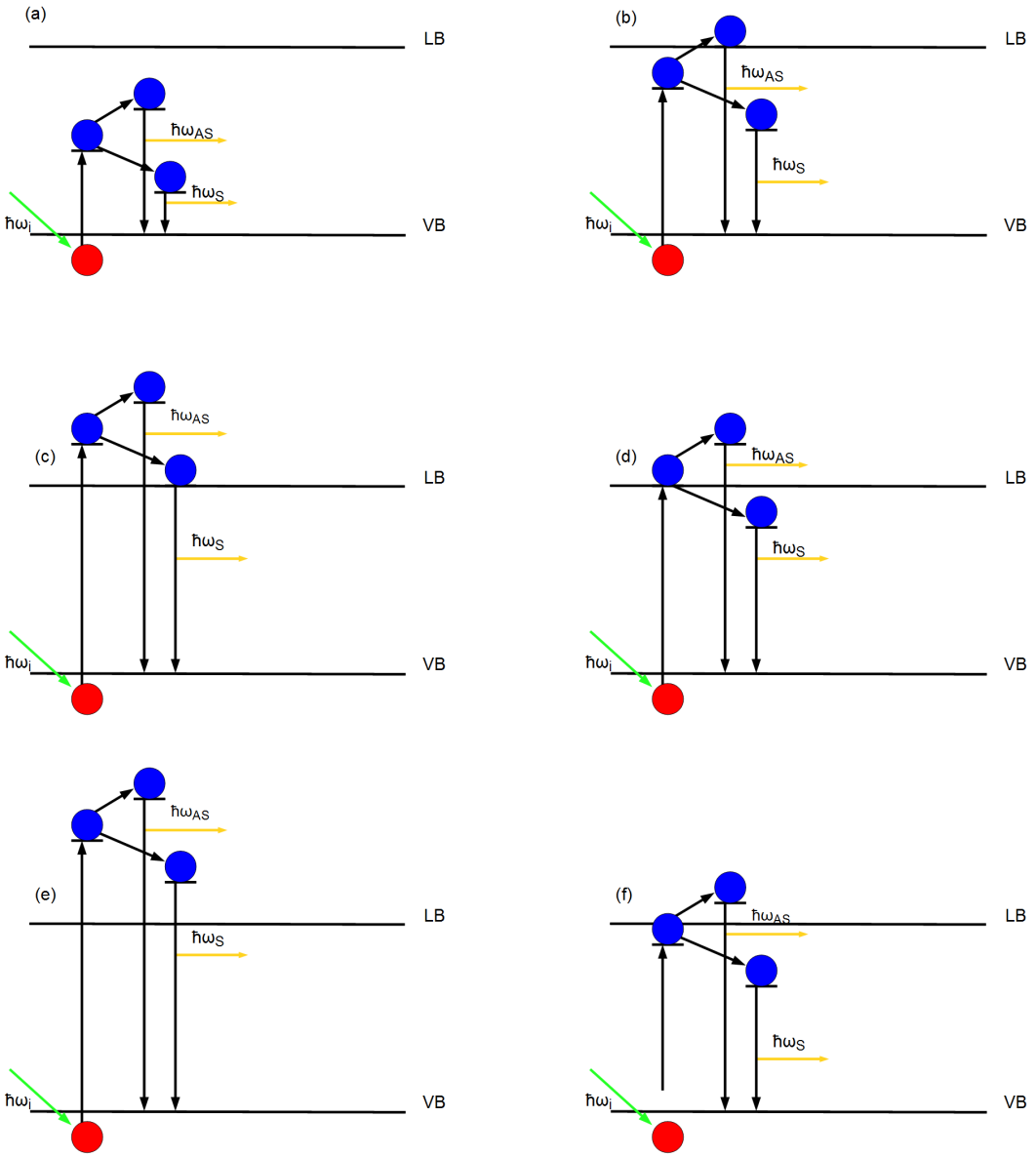

Fig. 3.4.: Dependence of the Raman process on the energy of the incoming photon. The red circles indicate the holes, the blue circles the electrons. The first electron (left) is always in state $|a\rangle$, the second (right) in $|b\rangle$. The green arrow indicated the incoming photon, the yellow light the outgoing photon for the Stokes/anti-Stokes process respectively.

4. Conclusion

For the investigated samples of Si, CaF_2 and graphite, the Stokes and anti-Stokes shifted Raman peaks were determined. Their position was measured and the Raman shift, energy and the ratio between the intensities of Stokes and anti-Stokes and Stokes and Rayleigh respectively were calculated. From the ratio of Stokes and anti-Stokes intensity, the temperature of the samples were determined. The gained data can be found in table 4.1.

The experimental and theoretical values for the phonon energy and wavenumber respectively are compatible with the theoretical predictions. For Si and CaF_2 the values are within one error interval, for graphite within three error intervals.

Sample	$E_{Ph}/[meV]$		$\lambda^{-1}/[cm^{-1}]$		χ_{A-S}	$T/[K]$	χ_{S-R}
	Exp.	Theo.	Exp.	Theo.			
Si	64.2 ± 2.1	65	520.7 ± 18.0	521	0.15 ± 0.01	388 ± 13	$10^{-7} - 10^{-8}$
CaF_2	39.9 ± 2.2	39.8	321.4 ± 18.1	321	0.23 ± 0.02	315 ± 12	$10^{-8} - 10^{-9}$
Graphite	192.0 ± 1.1	195.9	1555.6 ± 8.8	1580	–	–	$10^{-8} - 10^{-9}$

Tab. 4.1.: Obtained and theoretical data for Si, CaF_2 and graphite.

The ratio between anti-Stokes and Stokes peak was used to calculate the temperature of the sample. This was not possible for graphite, because the anti-Stokes peak was outside the measured range. For Si a temperature of $388K$ was found. The temperature of CaF_2 was $315K$, so only slightly above room temperature. Due to the fact that the data was obtained by another group, only speculations for causes can be given. It is more likely to see the Raman shifted peaks for the Si sample thus it is possible that this sample was used for the adjustment of the beam. Thus the sample was exposed to the Laser beam for a long time, which lead to a heating of the sample. The CaF_2 was probably exposed to the Laser beam for a shorter time and thus not heated that much.

The intensity of the Rayleigh peak was significantly higher than of the Stokes peak for all three samples. This is consistent with the theoretical expectations, because inelastic scattering is not as likely as elastic scattering.

The comparison of the total intensities (cf. table 4.2) shows, that the Rayleigh process has nearly the same intensity for all three samples, whereas the intensity of the Stokes and anti-Stokes process differ greatly. The intensity for this processes is the largest for Si, considerably lower for CaF_2 and still lower for graphite. This can be explained with the consideration of section 3.4. The energy of the incoming photons is $\hbar\omega_i = 2.33eV$. The bandgap of Si is $E_{gap,Si} = 1.1eV$ [6] and of CaF_2 $E_{gap,CaF2} = 12eV$ [7]. Thus, Si

is one of the cases, which is not resonant but nevertheless more intense due to the fact that the intermediate states are within the valence band and therefore real states. The bandgap of CaF_2 is larger than the energy of the exciting phonons. Therefore all of the intermediate states are virtual and the lifetime is low, leading to a drastically lower intensity than in the case of Si. The case of Graphite is more complex and was the interest of research for over 30 years. It could be explained sufficiently only in 2004 by Reich and Thomsen [8].

process	Si	Graphite	CaF_2
Rayleigh	$1 \cdot 10^5$	$1 \cdot 10^5$	$2 \cdot 10^5$
Stokes	2300	370	465
Anti-Stokes	340	-	107

Tab. 4.2.: Intensity for different processes and samples in counts.

A. Silicon

The fit parameters of the Rayleigh, first order Stokes and anti-Stokes and second order Stokes peaks with a Lorentzian function can be found in table A.1. The corresponding plots are shown in figure Fig. A.1.

process	λ_0 [nm]	$\Delta\lambda$ [nm]	I_0 [count]	c [count]	I_{tot} [count]
Rayleigh	531.99 ± 0.01	0.30 ± 0.03	$(1.2 \pm 0.3) \cdot 10^5$	120 ± 20	$(1.1 \pm 0.1) \cdot 10^5$
Stokes	547.20 ± 0.01	0.18 ± 0.01	4050 ± 80	-50 ± 50	2300 ± 115
2^{nd} Order Stokes	560.81 ± 0.02	1.23 ± 0.08	220 ± 10	90 ± 11	860 ± 43
Anti-Stokes	517.68 ± 0.01	0.16 ± 0.01	663 ± 16	137 ± 9	340 ± 17

Tab. A.1.: Spectrum of Si(111)

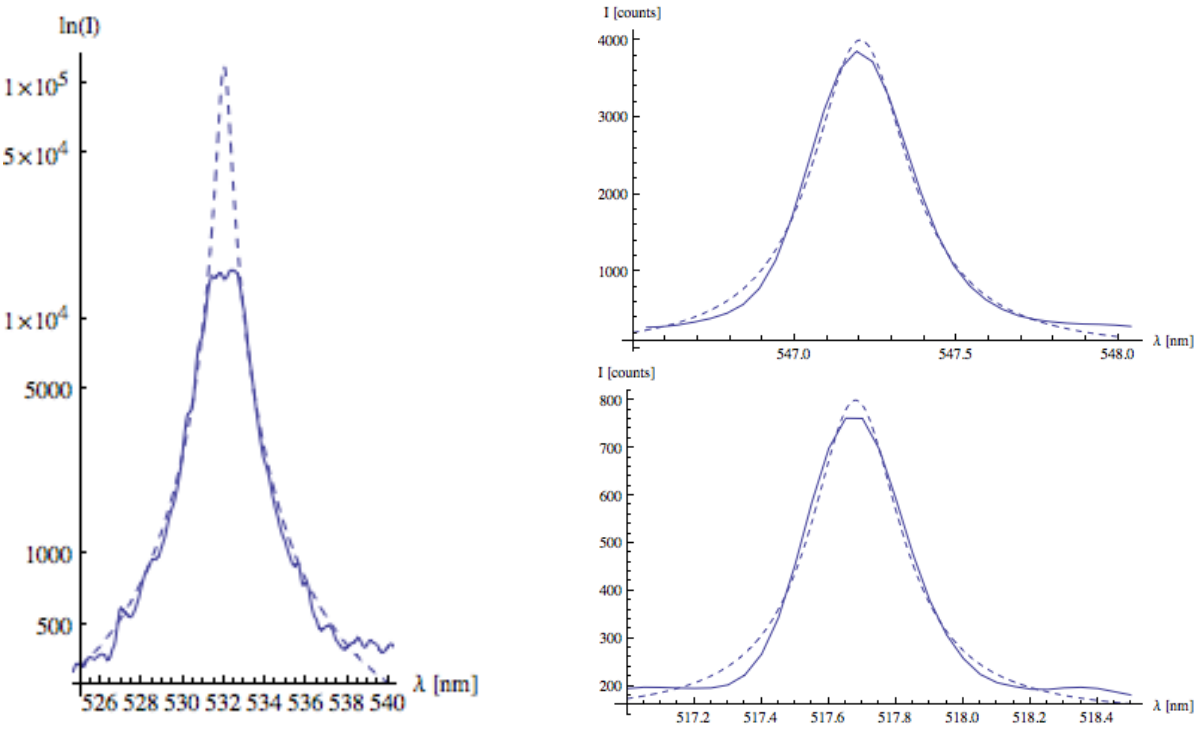

Fig. A.1.: Lorentzian fit of the Rayleigh (left), first order Stokes (top right) and first order anti-Stokes (bottom right) peak for Si.

B. Graphite

The fit parameters of the Rayleigh and first order Stokes peaks with a Lorentzian function can be found in table B.1. The corresponding plots are shown in Fig. B.1.

process	λ_0 [nm]	$\Delta\lambda$ [nm]	I_0 [count]	c [count]	I_{tot} [count]
Rayleigh	531.99 ± 0.01	0.25 ± 0.04	$(1.3 \pm 0.3) \cdot 10^5$	113 ± 7	$(1.0 \pm 0.1) \cdot 10^5$
Stokes	580.03 ± 0.01	0.12 ± 0.02	1040 ± 70	60 ± 40	370 ± 19

Tab. B.1.: Spectrum of Graphite

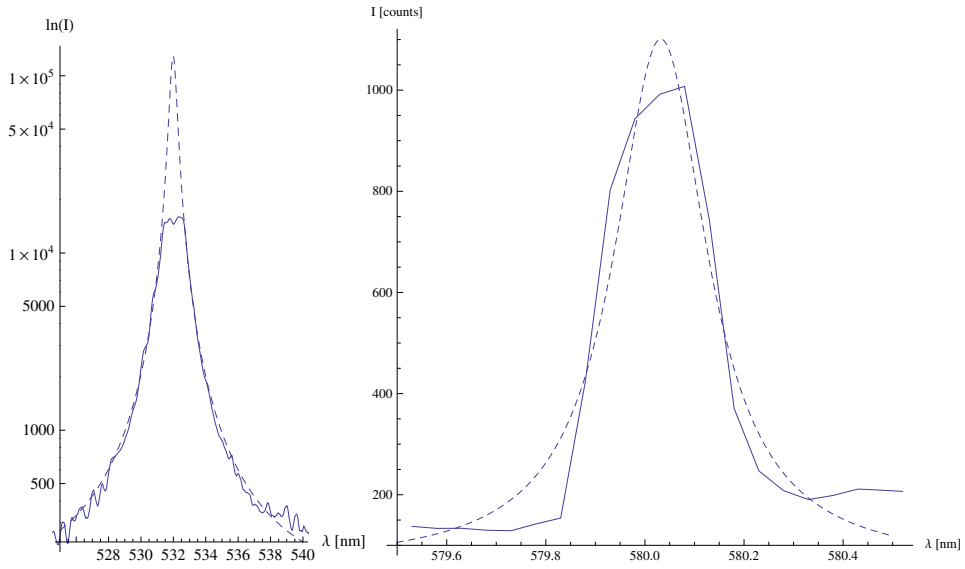

Fig. B.1.: Lorentzian fit of the Rayleigh (left) and first order Stokes (right) peak for graphite.

C. CaF_2

The fit parameters of the Rayleigh, first order Stokes and first order anti-Stokes peaks with a Lorentzian function can be found in table C.1. The corresponding plots are shown in Fig. C.1.

process	λ_0 [nm]	$\Delta\lambda$ [nm]	I_0 [count]	c [count]	I_{tot} [count]
Rayleigh	531.99 ± 0.01	0.1 ± 0.2	$(1.3 \pm 0.4) \cdot 10^6$	170 ± 10	$(2.3 \pm 0.2) \cdot 10^5$
Stokes	541.30 ± 0.01	0.21 ± 0.01	670 ± 10	270 ± 5	465 ± 24
Anti-Stokes	523.07 ± 0.01	0.16 ± 0.01	212 ± 6	203 ± 6	107 ± 6

Tab. C.1.: Spectrum of CaF_2

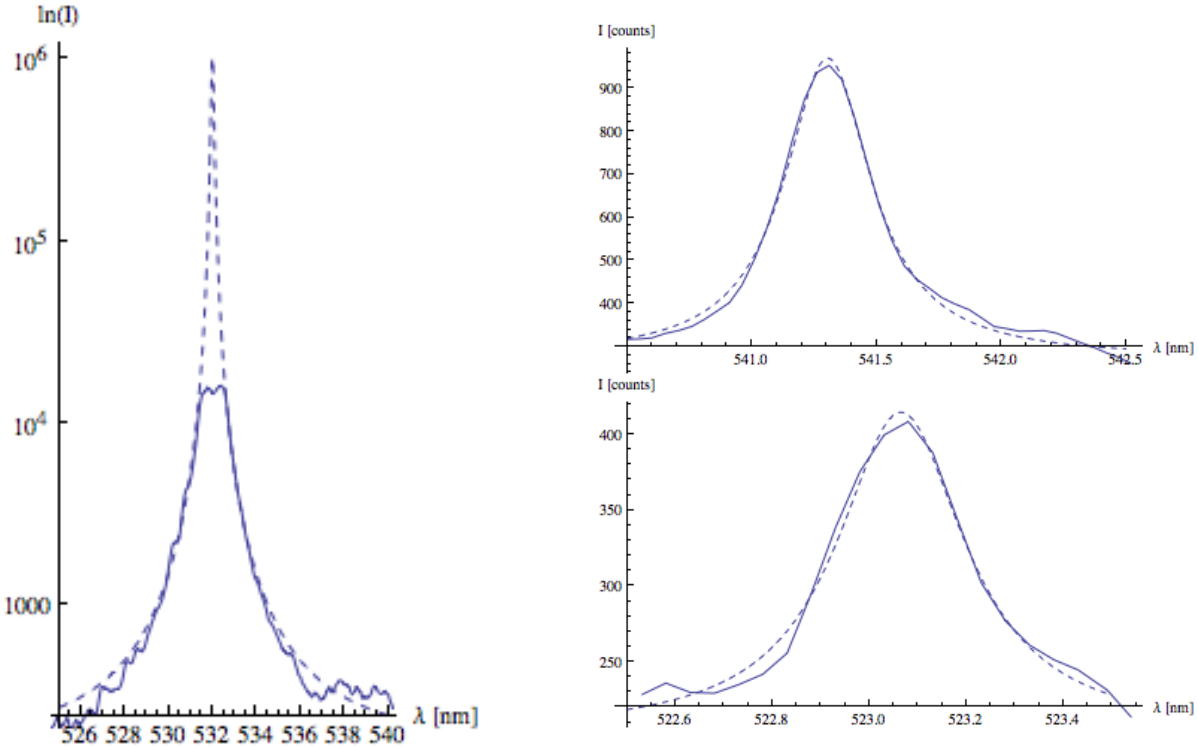

Fig. C.1.: Lorentzian fit of the Rayleigh (left), first order Stokes (top right) and first order anti-Stokes (bottom right) peak for CaF_2.

Bibliography

[1] Kopitzki, Konrad; *Einführung in die Festkörperphysik*; 2nd Edition; Teubner-Studienbücher Physik; Stuttgart; 1989

[2] Ibach, Harald; Lüth, Hans; *Festkörperphysik*; 7th Edition; Springer Verlag; 2008

[3] Yu, Peter; Cardona, Manuel; *Fundamentals of Semiconductors*; 4th Edition; Springer Verlag; 2010

[4] Fumagalli, Paul; *Notes from the lecture Festkörperphysik*; FU Berlin; Wintersemester 2010/2011

[5] *Ma 7 - Raman Scattering*; Instructions for the Advanced Laboratory Course at Freie Universität Berlin; 2011

[6] Streetman, Ben; Banerjee, Sanjay; *Solid State Electronic Devices*; 5th Edition; Prentice Hall; 1999

[7] Viernow, J. et al.; *Linear arrays of CaF_2 nanostructures on Si*; Appl. Phys. Lett., Vol. 74, No. 15; 1999

[8] Reich, Stephanie; Thomsen, Christian;*Raman spectroscopy of graphite*; Phil. Trans. R. Soc. Lond. A 362, 2272-2288; 2004